The Open Civil Engineering Journal
DOI: 10.2174/0118741495495426110207022l, 2026, 20, e187414954954
ISSN: 1874-1495
1

RESEARCH ARTICLE OPEN ACCESS

Contribution to the Micromechanical Analysis of Oedometric Modulus and Damping Ratio in Granular Compression Wave Propagation in Granular Medium

Said Derbane[1,*] and Hillal Ayas[2]

[1]*Department of Civil and Hydraulic Engineering, Faculty of Science and Technology, University of Jijel18000, Algeria*
[2]*Department of Structures and Materials, Civil Engineering Faculty, University of Sciences and Technology Houari Boumediene, B. P. 32 El Alia, Bab Ezzouar, Algiers16111, Algeria*

Abstract:

Objective: This study investigates the micromechanical behaviour of compression wave propagation in granular media using the Discrete Element Method (DEM), with a focus on the evolution and degradation of the oedometric modulus and the damping ratio under harmonic excitation.

Methods: A C++ DEM model was developed to simulate wave propagation in a granular deposit subjected to base excitation. The formulation explicitly incorporates nonlinear contact mechanics, interparticle friction, and energy dissipation under rigid-base, free-surface, and horizontal periodic boundary conditions. A three-phase loading protocol, comprising a 4.5-second amplitude ramp-up, a 6-second steady-state harmonic phase, and a 1.5-second ramp-down phase, was used to distinguish transient and steady-state responses across varying deformation amplitudes and confining pressures.

Results: The results demonstrate significant degradation of the oedometric modulus and a progressive increase in the damping ratio with increasing deformation amplitude, whereas higher confining pressures enhance the overall stiffness of the granular deposit. Compression waves exhibit lower damping and less degradation of the oedometric modulus than shear waves. Quantitatively, the free-vibration analysis provides an upper-bound estimate of stiffness with a fundamental frequency of 59.62 *rad/s*, a wave velocity of 20.49 *m/s*, and a maximum quasi-elastic modulus of 83.8×10^4 *Pa*. Conversely, the secant modulus derived from low-amplitude stress-strain hysteresis loops yields lower values of 82.7×10^4 *Pa*, inherently accounting for interparticle sliding and frictional dissipation, thus indicating that stiffness degradation initiates at sub-yield strain levels.

Discussion: In contrast to continuum-based approaches, this discrete framework elucidates the grain-scale mechanisms underlying the macroscopic dynamic behaviour of granular materials, highlighting the critical influence of the evaluation procedure on the determination of nonlinear soil parameters.

Conclusion: The DEM model provides a micromechanical interpretation of compression wave propagation in granular soil. Free-vibration analysis provides an estimate of elastic stiffness, whereas hysteresis loops capture dissipative mechanisms and consequently yield lower stiffness estimates. This distinction is important for geotechnical and seismic response analyses.

Keywords: DEM, Compression wave propagation, Oedometric modulus, Damping ratio, Micromechanical model.

© 2026 The Author(s). Published by Bentham Open.
This is an open access article distributed under the terms of the Creative Commons Attribution 4.0 International Public License (CC-BY 4.0), a copy of which is available at: https://creativecommons.org/licenses/by/4.0/legalcode. This license permits unrestricted use, distribution, and reproduction in any medium, provided the original author and source are credited.

*Address correspondence to this author at the Department of Civil and Hydraulic Engineering, Faculty of Science and Technology, University of Jijel 18000, Algeria; Tel: +213-6-6191-1155; Email: said.derbane@univ-jijel.dz

Cite as: Derbane S, Ayas H. Contribution to the Micromechanical Analysis of Oedometric Modulus and Damping Ratio in Granular Compression Wave Propagation in Granular Medium. Open Civ Eng J, 2026; 20: e187414954954.
http://dx.doi.org/10.2174/0118741495495426110207022 1

Received: April 26, 2026
Revised: June 25, 2026
Accepted: July 13, 2026
Published: November 13, 2026

Send Orders for Reprints to
reprints@benthamscience.net

1. INTRODUCTION

The mechanical behaviour of discrete granular materials subjected to various types of dynamic loading, particularly during the propagation of longitudinal elastic compression waves, is an important topic that warrants further investigation. This is primarily due to the complexity of interactions between localised force fields generated at individual contact points and the macroscopic behaviour of the granular assembly. Moreover, traditional continuum-based modelling techniques can capture only a limited number of these aspects, often neglecting important features such as grain-scale contact mechanics, stiffness degradation, and energy dissipation [1].

In contrast to continuum methods, the Discrete Element Method (DEM) enables the simulation of the mechanical behaviour of granular assemblies, with explicit consideration of both the individual grain characteristics and contact interactions among them [2]. In addition to accurately simulating the wave propagation process within granular materials, DEM allows the influence of different types of energy loss mechanisms occurring at particle contacts to be assessed. These mechanisms contribute significantly to the overall energy dissipation observed in granular systems. Previous investigations have shown the potential of DEM in evaluating several mechanical aspects related to the static and dynamic behaviour of granular materials, including stress–strain relationships, grain rearrangements and attenuation of waves passing through a layer of grains [3, 4]. The former property represents one of the most significant parameters used to assess the compressibility of granular materials, depending upon various factors, such as the history of applied stresses, grain arrangement and configuration, and the adopted contact stiffness values [5]; similarly, the latter is directly related to the mechanisms of energy loss at grain-to-grain contacts, including frictional losses and losses associated with inelastic deformation [6]. Specifically, recent micromechanical studies have successfully captured a wide range of complex phenomena, including stick-slip behaviour under varying pressures [7], pile penetration mechanics [8], and the direct influence of grain shape on stress-dilatancy parameters [9]. Furthermore, advanced DEM applications have been extended to multiphysical problems, such as fluid-particle interaction during seepage erosion [10] and the axial response of buried pipelines [11]. To better capture the micromechanical response and wave dynamics in soils, several discrete element models have been proposed. Recent investigations on compression wave propagation and energy absorption in dry sandy soil were carried out as reported previously [12], building upon earlier DEM analyses of stress-wave responses in particle assemblies under triaxial loading [13]. Furthermore, the micro-macro response of sand subjected to loading conditions was investigated [14], while a discrete-based multi-scale modelling approach was developed in another study [15] to evaluate seismic wave propagation. Nonetheless, several questions remain open regarding the degradation of the oedometric modulus and changes in damping when a granular assembly is subjected to repeated cycles of compression waves. Many studies have dealt with the evaluation of both the oedometric modulus and damping in granular materials, whereas much less attention has been paid to their evolution under dynamic loading. Furthermore, the majority of previous studies on wave propagation in granular media have focused predominantly on shear waves, leaving compression waves comparatively less explored. Therefore, DEM appears to be a useful tool for investigating these aspects. To provide a comprehensive background on recent advances in computational granular dynamics and advanced numerical modelling of dynamic soil behaviour over the past decade, a systematic literature review is presented in Table **1**.

The literature reviewed above highlights a clear trend: although the Discrete Element Method (DEM) has been widely adopted to study the behaviour of granular soils under cyclic loading, almost all existing research has focused on shear-wave propagation (Vs) and shear modulus degradation (G/G_0). This strong bias leaves a significant gap in the understanding of longitudinal compression-wave propagation, particularly regarding its relationship with the oedometric modulus (E) and damping ratio (ξ) under vertical dynamic loading conditions. Most traditional models do not account for the non-destructive elastic threshold and therefore neglect the evolution of interparticle friction required to capture the onset of nonlinear behaviour. Consequently, the mechanisms governing energy dissipation and stiffness variations under purely vertical dynamic loading require further investigation to gain a better understanding of these phenomena.

Table 1. Literature review on numerical modelling in the dynamic behaviour of soils with a micromechanical investigation.

Reference	Methodology	Main Conclusions	Work Limitations	Relevance to the Present Study
Tang and Yang [4]	Advanced numerical simulations exploring the explicit role of non-spherical particle shapes, microstructural interlocking, and contact geometry on elastic wave propagation.	Particle shape anisotropy and surface non-sphericity significantly alter internal force chain paths, wave velocities, and localized energy transmission.	The study mainly deals with wave velocity and directional scattering under free-boundary impulses, without quantifying the cyclic degradation of the oedometric modulus or compression damping loops.	Justifies the consideration of detailed interparticle interactions (sliding and friction) and microstructural confinement to accurately track the responses of compression waves (V_p).
Ozbay and Cabalar [7]	Triaxial laboratory testing combined with discrete numerical modelling to investigate stick-slip friction mechanisms under cyclic shear.	The increase in triaxial confining pressure and varying strain rates are directly related to stick-slip amplitude dynamics.	The study focuses on large-deformation shear failure and stick-slip friction instabilities rather than non-destructive longitudinal wave propagation parameters.	Justifies our interest in low strain and provides insights into how confinement pressure alters stability.
Gezgin *et al.* [8]	Three-dimensional discrete element modelling designed to isolate and analyse the distinct influences of individual soil characteristics under high-penetration boundary conditions.	Stiffness, interparticle friction, rolling friction, and packing density were found to govern the development of macroscopic limit forces.	The study focuses on high-deformation, monotonic pile penetration mechanics and localized particle displacements rather than non-destructive cyclic elastic wave velocities.	The micromechanical parameters considerably influence the overall assembly stabilisation under strict boundary constraints.
Arda and Cinicioglu [9]	Investigating the explicit influence of grain shape (sphericity and angularity) on stress-dilatancy relationships in granular assemblies.	High particle angularity increases peak shear strength and shifts the critical state line, significantly modifying interlocking and dilatancy parameters.	The study focuses on quasi-static, monotonic triaxial shear paths and stress-dilatancy behaviors rather than non-destructive cyclic compression-wave damping.	It offers a valuable framework for understanding how grain geometry and microstructural interlocking dictate the initial packing state, establishing stable contact configurations prior to dynamic testing.
Cheng *et al.* [10]	Coupled CFD-DEM modelling investigating the influence of irregular coarse particle shapes (spherical, cubic, tetrahedral, and ellipsoidal) on seepage erosion and pore-network evolution in gap-graded soils.	Non-spherical particle shapes lower pore-topology connectivity, increase resistance to fine-particle transport, and critically govern the magnitude of internal erosion.	The study focuses on fluid-particle interaction, high-strain mass loss, and hydraulic seepage erosion rather than non-destructive cyclic stress-wave propagation or elastic stiffness.	Highlights how irregular grain shapes and aspect ratios significantly alter internal fabric topology, supporting the focus on micromechanical packing stability.
Guo *et al.* [11]	Discrete element modelling investigating the macro-micro axial interaction, force transfer mechanisms, and soil-pipe behaviour of pipelines buried in unsaturated coarse-grained soils.	Matric suction, moisture distribution, and particle-pipe contact dynamics significantly govern axial pulling resistance and localized failure zones around the structure.	The study focuses primarily on large-strain structural displacement, pipeline slip, and unsaturated soil suction mechanics rather than non-destructive cyclic elastic-wave velocities.	The robustness of DEM in modelling complex soil-structure contact constraints provides a valuable comparative framework for rigid boundary interactions.
Cui *et al.* [12]	Coupled numerical and experimental analysis investigating compression-wave propagation velocity and kinetic energy absorption characteristics in dry sandy soils.	The study confirmed that compression-wave velocity scales with confinement and packing density, while energy absorption is driven by macroscopic damping.	The study does not compare or quantify the differences between modulus values derived *via* free-vibration states and those extracted from the slopes of cyclic stress-strain curves.	The originality of this work lies in the development of a dual evaluation approach based on free vibrations and hysteresis loops.
Li *et al.* [13]	DEM simulation exploring the behaviour of anisotropic granular packing geometries subjected to multi-directional shearing paths.	Particle morphology and contact networks govern directional fabric evolution and induce macroscopic stiffness anisotropy.	The study focuses primarily on triaxial shear loading configurations, leaving the rigid lateral boundary constraint typical of oedometric compression unexamined.	It provides a valuable microstructural benchmark for analysing how contact-network fabrics and contact-normal distributions evolve under initial confinement.
Ezzeddine *et al.* [14]	Micromechanical DEM tracking of contact-force variations, particle sliding, and oedometric modulus evolution under cyclic loading.	The study revealed that macro cyclic hysteresis loops, modulus variation, and energy dissipation are driven by the micro-slip threshold of the contact networks.	The study focuses on macro-micro cyclic deformation and modulus degradation paths without quantifying the specific wave velocity or damping of dynamic compression waves.	The study provides a direct comparative benchmark for validating our cyclic oedometric modulus curves and interpreting their micromechanical origins at low amplitudes.
Mohamed *et al.* [15]	Discrete-based multi-scale simulation exploring longitudinal and shear wave propagation profiles under seismic excitations.	The study confirmed that macroscopic seismic wave attenuation correlates closely with microstructural contact force chains and particle-slip events across varying soil depths.	The model was calibrated and validated for shear wave velocity profiles, leaving the specific compression wave response and its evolution unquantified.	A multi-layer macroscopic recording framework was implemented across independent tracking intervals to ensure a consistent methodology for analysing wave propagation throughout the granular assembly.

To address this gap, the present study analyses the behaviour of a non-cohesive granular deposit subjected to dynamic excitation at its base using a two-dimensional discrete element model. A harmonic base displacement is imposed to simulate the propagation of compression waves through a granular assembly of circular particles. By monitoring particle-scale interaction under these dynamic conditions, this study highlights the microstructural modifications and contact-force redistributions that govern stiffness degradation (*i.e.*, the degradation of oedometric modulus (E)) and energy dissipation (*i.e.*, the evolution of damping ratio (ξ)) as a function of strain level. Particular emphasis is placed on identifying the critical threshold above which nonlinear behaviour becomes dominant. Ultimately, this study aims to provide a practical framework for improving the prediction of the micromechanical compression response of granular media in engineering applications, thereby bridging the gap between grain-contact mechanics and macroscopic soil behaviour.

2. MATERIALS AND METHODS

2.1. Discrete Element Method (DEM) for Modelling Granular Materials

The Discrete Element Method (DEM) used in this study is based on the principles of molecular dynamics, with translational and rotational motion governed by Eqs. (**1** and **2**) (Fig. **1**) [16].

All the physical and micromechanical parameters governing the model and used in this study are listed in the **Appendix**.

For a grain i, let its centre of mass be denoted by C_i, its radius by r_i, its position vector by $\vec{x}_i = \overrightarrow{OC_i}$, and its angular velocity by $\vec{w}_i = \frac{d\vec{\varphi}_i}{dt}$. The translational velocity of the grain is denoted by $\vec{v}_i = \frac{d\vec{x}_i}{dt}$. The contact point between two grains is denoted by C.

$$m_i\ddot{\vec{x}}_i = \sum_j \vec{F}_{ij}^{contact} + m_i\vec{g} \quad \textbf{(1)}$$

The translational acceleration of a grain is denoted by $\ddot{\vec{x}}_i$, its mass by m_i, the interaction force exerted on grain j by a grain i in contact with it by $\vec{F}_{ij}^{contact}$, and the acceleration due to gravity by $\vec{g}$. The rotational equilibrium is given by Eq. (**2**):

$$I_i\ddot{\vec{\varphi}}_i = \sum_j \vec{M}_{ij}^{contact} \quad \textbf{(2)}$$

$\ddot{\vec{\varphi}}_i$ denotes the rotational acceleration of the grains, I_i is the moment of inertia, $\vec{M}_{ij}^{contact}$ represents the moments generated by the contact forces $\vec{F}_{ij}^{contact}$ about the centre of mass of the grain. Grain interactions occur at contact points, where each grain exchanges forces with its neighbouring grains. The overall strain of the medium is assumed to result primarily from the relative motions between grains, which are treated as rigid bodies. The contact force is calculated using Eq. (**3**) [17, 18].

$$\vec{F}_{ij}^{contact} = \vec{F}_n\vec{n} + \vec{F}_s\vec{s} \quad \textbf{(3)}$$

$\vec{F}_n$ and $\vec{F}_s$ are the normal and tangential contact forces, respectively. The use of a simple grain shape plays an important role in reducing computational time [17]. The most commonly used shapes are discs for two-dimensional (2D) modelling and spheres for three-dimensional (3D) modelling. The contact forces are calculated using simple models based on a slight overlap between grains.

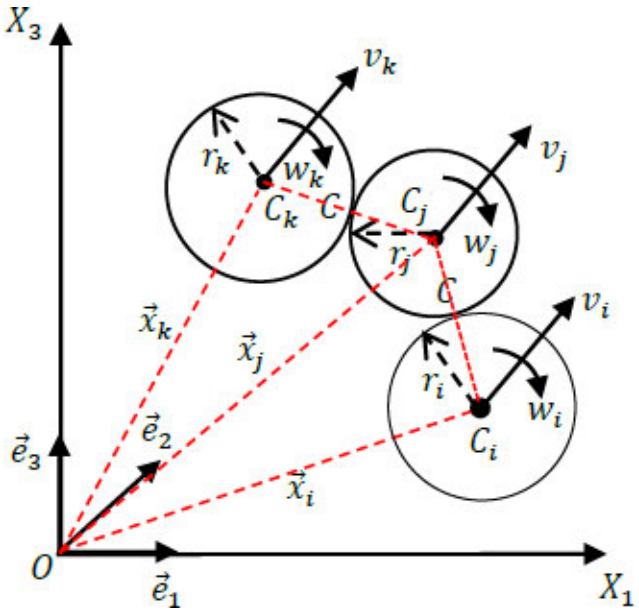


Fig. (1). Description of grain movement.

2.2. Contact Laws and Interaction Models

2.2.1. Contact Forces

A simplified decomposition is used to analyse the contact forces into a normal component, $\vec{F}_n$, and a tangential component, $\vec{F}_s$, lying in the plane tangent to the grain at the contact point. The normal force is described by a viscoelastic model, as shown in Fig. (**2a** and **b**).

The normal contact force $\vec{F}_n$ is calculated using Eq. (**4**) [19].

$$\vec{F}_n = (-k_n D_n - v_n V_n).\vec{n} \quad (4)$$

where k_n and v_n are the elastic constant and the viscous damping constant, respectively.

V_n denotes the normal velocity.

The calculation of the normal contact force between two grains depends on the normal contact distance, denoted by $D_n \leq 0$ (contact force calculation condition).

The normal distance D_n between i and j is defined geometrically by Eq. (**5**):

$$D_n = \left\|\vec{x}_j - \vec{x}_i\right\| - r_i - r_j \quad (5)$$

where r_i and r_j are the radii of grains i and j.

The tangential contact force between two grains is computed using a viscoelastic model with friction (Fig. **3**).

The tangential contact force, $\vec{F}_s$, is given by Eq. (**6**) as follows [20]:

$$\vec{F}_s = min(k_s D_s + v_s V_s, \mu_d F_n)\vec{s} \quad (6)$$

where k_s is the tangential stiffness, v_s is the viscous damping coefficient, μ_d is the inter-particle coefficient of friction, and the relative tangential displacement is given by Eq. (**7**):

$$D_s = \sum_{dt} V_s dt \quad (7)$$

The tangential velocity of grain j with respect to grain i is given by Eq. (**8**):

$$V_s = (V_j - V_i)\vec{s} \quad (8)$$

If the tangential force $F_s >$ to $\mu_s F_n$ reaches the Coulomb static friction threshold, the grains enter the sliding regime, F_s set to F_s^{min}. At this point, the tangential spring deformation must be adjusted to be consistent with the kinetic friction force, which is given by Eq. (**9**):

$$D_s = \frac{F_s^{min}}{k_s} \quad (9)$$

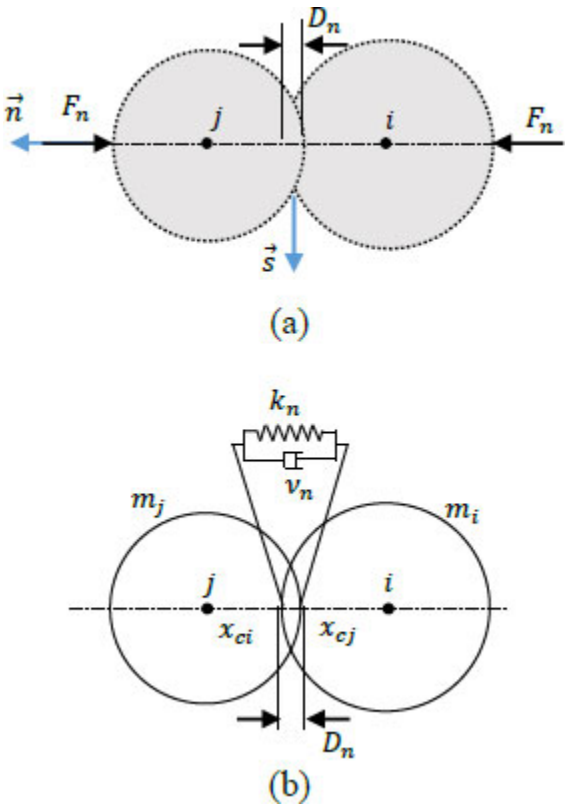


Fig. (2). Normal contact force between particles: (**a**) Physical model; (**b**) viscoelastic model.

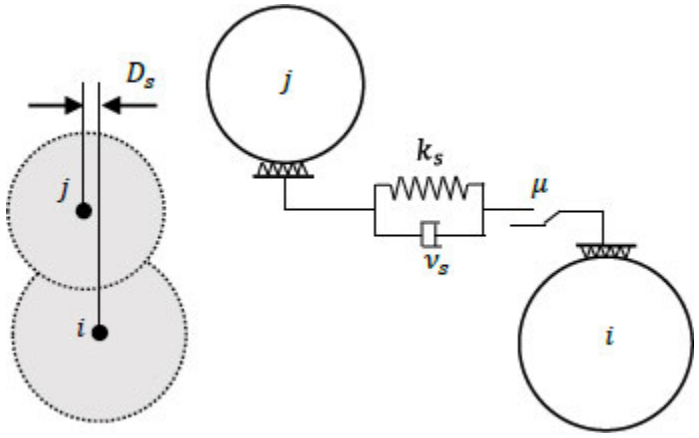


Fig. (3). Tangential contact force between grains.

It should be noted that the lower limit of the friction force F_s^{min} is expressed by Equation (**10**) as follows:

$$F_s^{min} = (2\mu_d - \mu_s)\, F_n \quad \textbf{(10)}$$

where: μ_s and μ_d are the static and dynamic coefficients of friction, respectively.

To account for the damping of the rolling motion of natural grains, a rolling resistance M_r is incorporated into the model. The rolling resisting moment is assumed to result from the eccentricity of the normal contact force, as illustrated in Fig. (**4**). Therefore, it is calculated using Eq. (**11**) as follows [21]:

$$M_r = F_n . b_r \quad \textbf{(11)}$$

where $b_r = \alpha.\beta,\ \ \beta = \sqrt{r^2 - (r + \frac{D_n}{2})^2}$, and 0 < α < 1; α is fixed at 0.5 in this study.

2.2.3. Contact Duration and Time-Step Integration

It is important to note that, to accurately capture the evolution of the normal and tangential contact forces, the time step must be much smaller than t_c ($\Delta t << t_c$). A common practice is to set $\Delta t \approx t_c/10$. For a viscoelastic contact model, the contact duration tc can be approximated using Eq. (**12**):

$$t_c = \pi \sqrt{\frac{m_{eff}}{k_n}} \quad \textbf{(12)}$$

where $m_{eff} = \frac{m_i . m_j}{m_i + m_j}$ is the effective mass and k_n is the normal stiffness. Accordingly, the maximum allowable time step is given by Eq. (**13**):

$$\Delta t_{max} \approx 0.1\pi \sqrt{\frac{m}{k_n}} \quad \textbf{(13)}$$

where m is the smallest effective mass in the system.

2.3. Analytical Solutions of Wave Propagation in Soil

For a homogeneous, linearly elastic, isotropic soil profile, the one-dimensional (1D) differential equation governing the displacement $u(z,t)$ is given by Eq. (**14**) [22]:

$$V_p^2 \frac{\partial^2 u}{\partial z^2} = \frac{\partial^2 u}{\partial t^2} \quad \textbf{(14)}$$

where u is the vertical displacement and V_p is the compression-wave velocity, given by Eq. (**15**):

$$V_p = \sqrt{\frac{E}{\rho}} \quad \textbf{(15)}$$

where E is the oedometric modulus of the soil, and ρ is its mass density.

For harmonic excitation, the solution is obtained using Eq. (**16**):

$$u(z,t) = \frac{u_o V_p}{E\omega} \frac{(\sin\frac{\omega}{V_p} z)}{\cos(\frac{\omega}{V_p} h)} . \sin \omega t \quad \textbf{(16)}$$

where u_o is the excitation amplitude, ω is the excitation frequency, h is the soil layer depth, and z is the depth coordinate.

2.4. Numerical Model DEM

In this study, a two-dimensional (2D) simulation of compression-wave propagation in a granular soil profile is conducted using the Discrete Element Method (DEM). The soil grains are deposited under gravity to form a dense granular assembly. Several boundary conditions are implemented: periodic boundary conditions are applied laterally to simulate an infinite horizontal extent, the top surface is left free, and the base is supported by a rigid wall representing the bedrock. To generate wave motion, a chain of grains is placed directly on the bedrock, and a controlled horizontal harmonic displacement is applied to this chain. A vertical load may also be applied to the top surface to adjust the stiffness of the profile and to simulate the behaviour of deeper soil layers. The interaction laws between the grains are described in Section 2.2.

The interaction laws between the grains in the chain and those in the soil profile are identical to those governing grain-to-grain interactions within the profile.

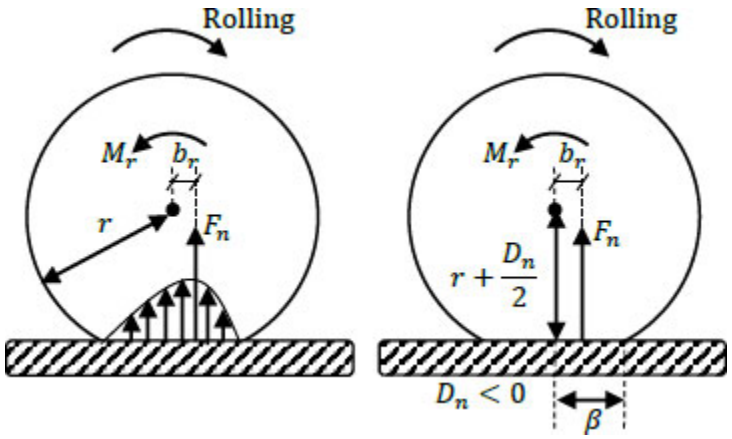


Fig. (4). Rolling resistance model.

To analyse wave propagation, a harmonic excitation with a prescribed amplitude and frequency is applied to the grain chain at the base of the soil profile. The soil profile is divided into several horizontal layers, and the average displacement within each layer is recorded throughout the excitation to evaluate the wave transmission characteristics.

2.5. Simulation Parameters

Figure **5** illustrates the granular soil profile model subjected to excitation, together with the applied boundary conditions. The physical properties of the grains and the micromechanical parameters used to calculate the contact forces are summarised in Table **2** [23-29].

The soil profile is generated by pluviating 5000 grains under gravity, resulting in a dense assembly stabilised within a domain measuring 2.0 *m* in width and 0.54 *m* in depth. Once stabilised, the profile is subjected to a harmonic excitation defined by $u(t) = u_0 \sin(\omega t)$, where u_0 is the amplitude and ω is the angular frequency.

To minimise the effects of transient responses in the soil deposit, the excitation is applied in three phases, following the procedure proposed earlier [25]. During the first phase, the excitation amplitude is gradually increased from zero to the target steady-state value. In the second phase, the amplitude is held constant to induce steady-state oscillations. Finally, during the third phase, the amplitude is progressively decreased back to zero. In the simulations presented, the durations of these three phases are set to 4.5 seconds, 6 seconds, and 1.5 seconds, respectively. This staged loading strategy allows transient effects to decay substantially before the steady-state phase is reached. The results discussed below correspond primarily to this steady-state phase.

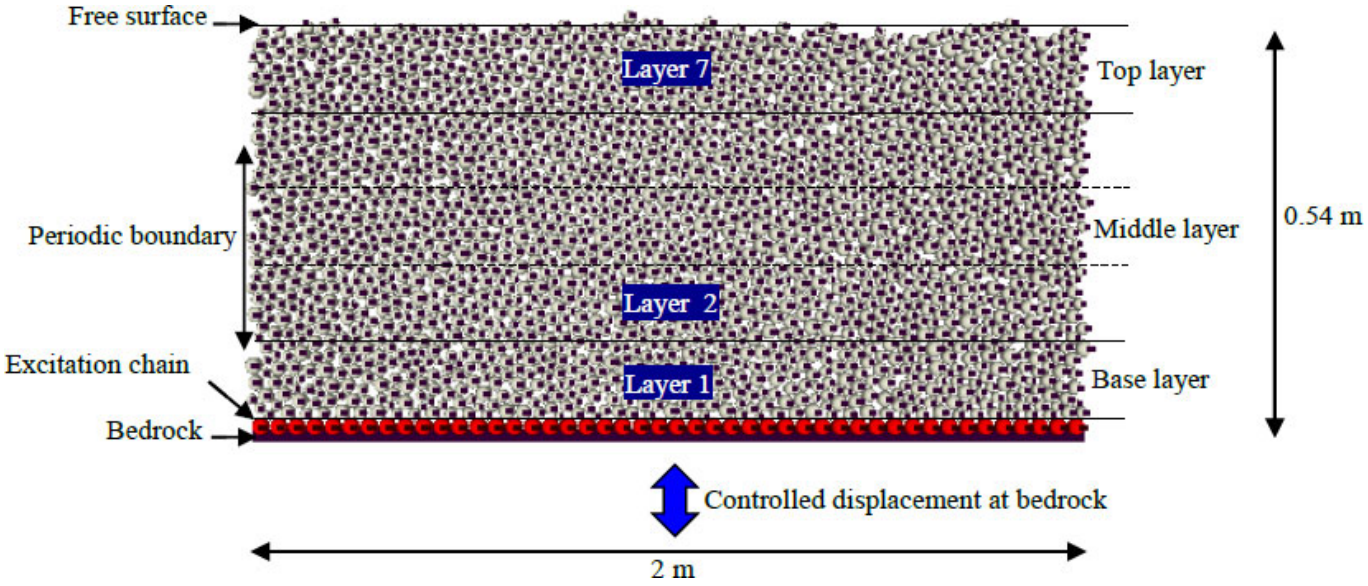


Fig. (5). Sand profile and boundary condition [23].

Table 2. Material properties and numerical simulation parameters.

Parameters	Value
Number of Grains	5000
Grains radii r_i	$1.00x10^{-3}$ *to* $2.00x10^{-3}m$
Density G_s	2600 kg/m^3
Normal intergranular stiffness k_n	$1.2\ x10^6 N/m$
Shear intergranular stiffness k_s	$9.6x10^5 N/m$
Intergranular friction coefficient μ	0.5
Normal viscous damping coefficient v_n	41.38 kg/s
Tangential viscous damping coefficient v_s	33.10 kg/s
Acceleration of gravity g	9.81 m/s^2

For the purposes of the analysis, the soil deposit is divided into seven horizontal layers, and the displacement recorded in each layer represents the average displacement of all grains within that layer.

To further clarify the simulation procedure using the Discrete Element Method (DEM), Fig. (**6**) illustrates the workflow, which is organised into three key calculation phases.

The granular deposit is generated using the gravitational pluviation technique. At the initial stage, the grains are arranged on a regular lattice without any initial contact. They are then released under gravity, allowing them to settle onto the rigid base that represents the bedrock.

Specifying 5000 grains in this model provides a balanced compromise, allowing the formation of a representative granular assembly while keeping computational costs manageable. The chosen particle radii and density are intended to represent the physical characteristics of a natural, medium-grained sand. The stiffnesses $\frac{k_n}{k_s}$ = 0.8 is commonly adopted in DEM simulations and reflects typical contact behaviour in granular materials. The interparticle friction coefficient of μ=0.5 is used to ensure realistic sliding behaviour consistent with dense granular materials. The normal and tangential damping coefficients (v_n and v_s) were selected to ensure numerical stability while preserving the dynamic response of the system without introducing excessive damping.

The excitation parameters are amplitude of u_0 = 4 x $10^{-4}m$ and angular frequency of ω=30 *rad/s*. During the first phase (*i.e.* from 0 to 4.5 *s*), the displacement amplitude is increased linearly with time from zero to 4 x 10^{-4} *m*. It is then maintained at this amplitude for 6 seconds and gradually decreased to zero over 1.5 *seconds*. Figure **7** shows the resulting bedrock displacement response.

3. RESULTS AND DISCUSSIONS

3.1. Free Vibration Response

Two techniques are used to estimate the maximum oedometric modulus. The first method involves determining this modulus from the pseudo-elastic oscillations observed during the free-vibration phase that follows the end of the excitation (Fig. **8**). For this method, the soil deposit is subjected to harmonic excitation with an amplitude of u_0 = 4 x $10^{-4}m$ and an angular frequency of 30rad/s. The second method involves determining the modulus from the hysteresis curves obtained at low excitation amplitudes.

From Fig. (**8**), the fundamental period can be estimated as approximately T = 0,1054 *seconds*. Hence, the fundamental frequency can be calculated using Eq. (**17**).

$$\omega_1 = \frac{2\pi}{T} \quad \textbf{(17)}$$

The calculated fundamental frequency is ω_1= 59.62 *rad/s*.

The compression wave velocity can be estimated from the fundamental period of the elastic oscillation using Eq. (**18**) [22]:

$$V_p = \frac{4h}{T} \quad \textbf{(18)}$$

Accordingly, the compression-wave velocity for the present soil deposit is V_p=20,49*m/s*.

Using Eq. (**15**), the oedometric modulus can be estimated as follows Eq. (**19**):

$$E_{0\,max} = V_p^2 . \rho \quad \textbf{(19)}$$

Upon calculation, the oedometric modulus is obtained as:

$E_{0_{max}}$ = $20,49^2$ x 1996,77 = 838326,322 *Pa*

Therefore: $E_{0_{max}} \cong 83.8 \times 10^4$ *Pa*

3.2. Estimation of Oedometric Modulus E_0

In this section, the maximum oedometric modulus E_0 is evaluated. This value corresponds to the slope of the hysteresis curves at low excitation amplitudes, on the order of 10^{-5}.

The equivalent oedometric modulus was determined from the slopes of the mean stress–strain hysteresis loops for each loading cycle, following the procedure described in Eq. (**20**).

$$E = \frac{\sigma_{y\,cyc}}{\varepsilon_{y\,cyc}} \quad \textbf{(20)}$$

where:

$$\sigma_{y\,cyc} = \frac{\sigma_{y\,cyc3} + \sigma_{y\,cyc4} + \sigma_{y\,cyc5}}{3} \quad \textbf{(21)}$$

where σ_y *cyc* and ε_y *cyc* are defined by Eqs. (**21** and **22**), respectively, representing the average cyclic compressive stress and strains. The terms $\sigma_y\ cyc_3$, $\sigma_y\ cyc_4$, and $\sigma_y\ cyc_5$ refer to the compressive stresses in the third, fourth, and fifth sub-layers, respectively.

$$\varepsilon_y = \frac{u_6^p - u_1}{y_6 - y_1} \quad \textbf{(22)}$$

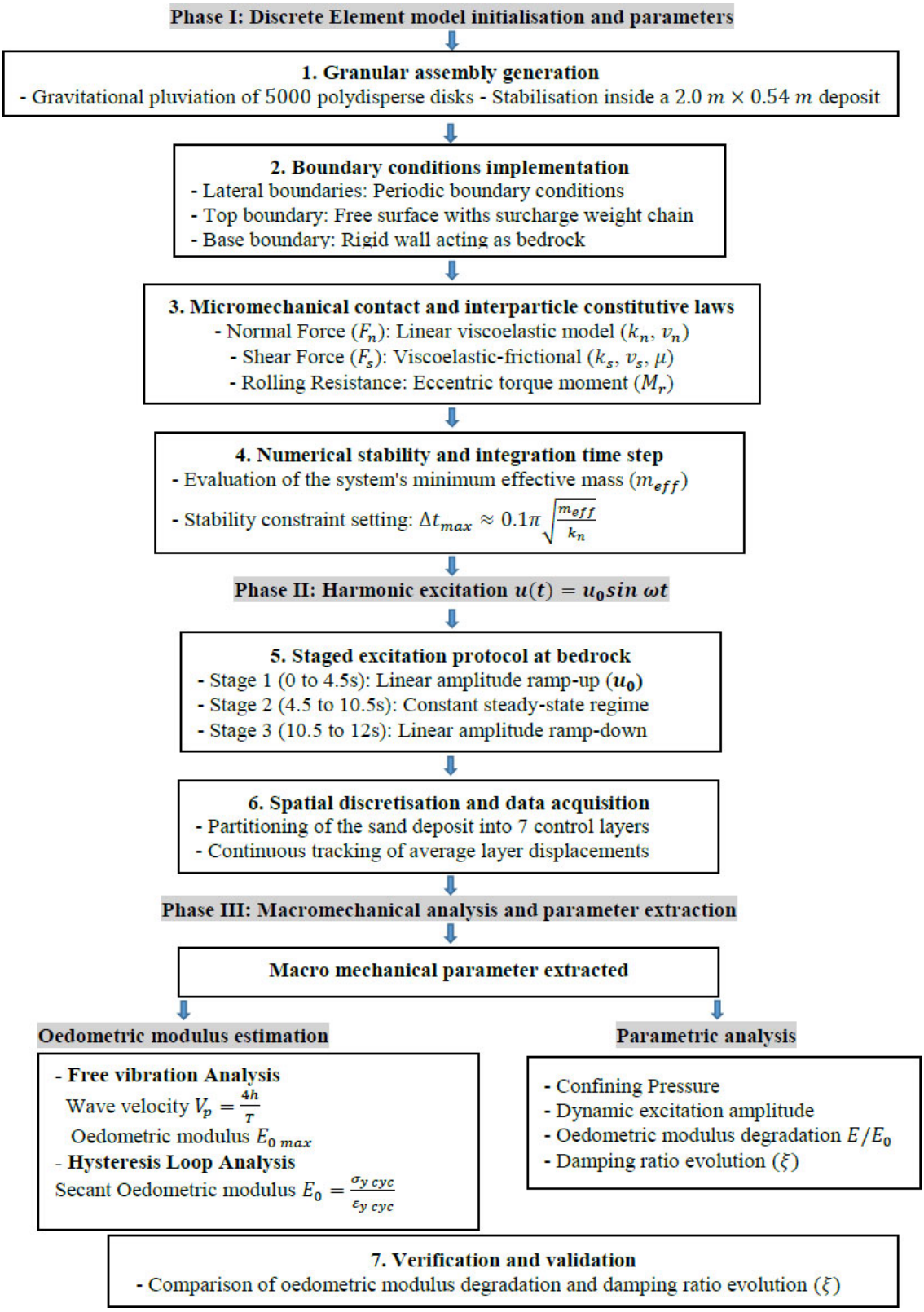


Fig. (6). Methodological flow chart.

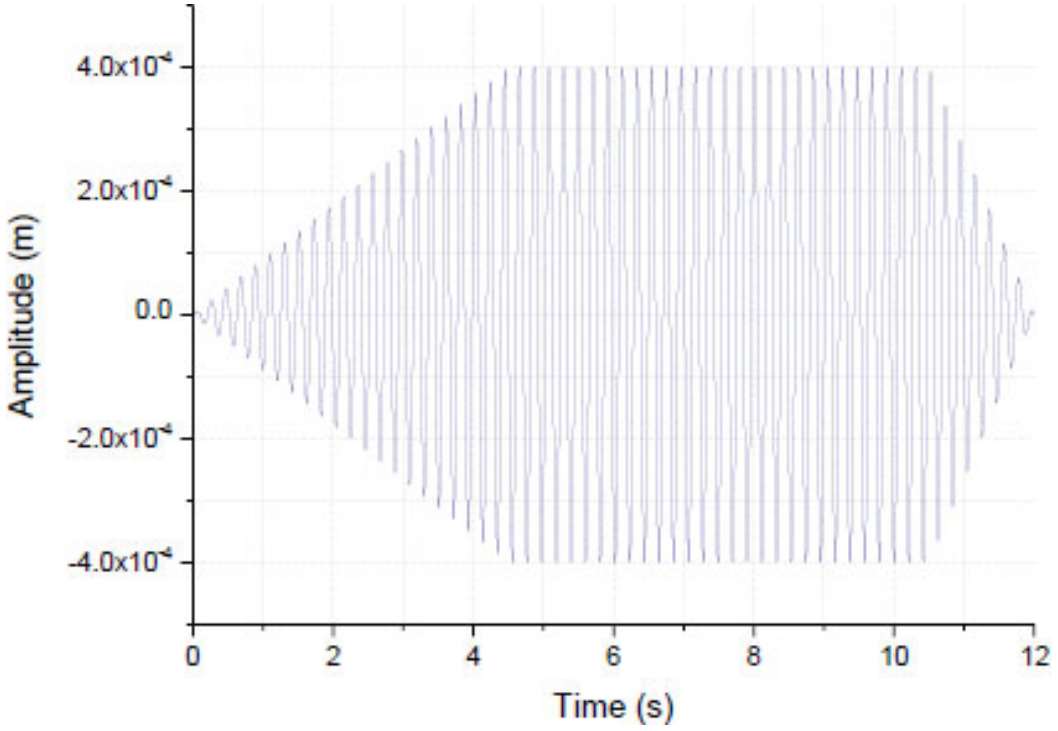


Fig. (7). Bedrock displacement response (excitation).

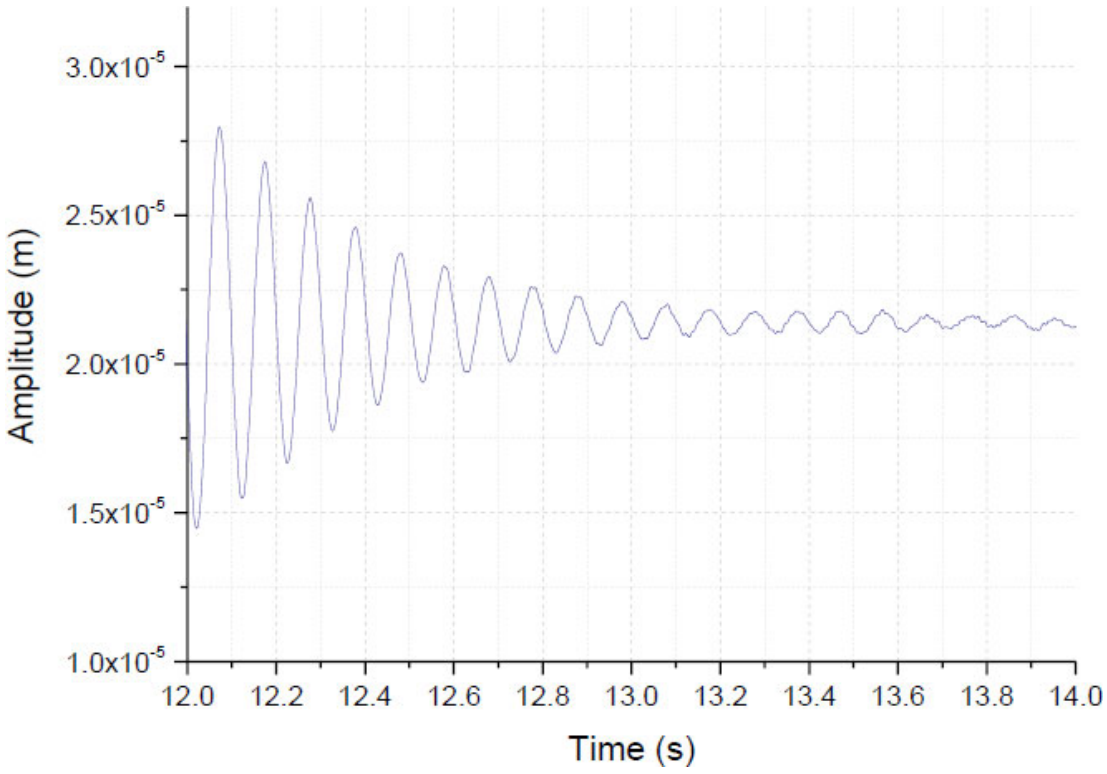


Fig. (8). Detailed view of the displacement response in the top layer during free vibration (after 12 seconds).

In this expression, u^{p}_{6} represents the peak displacement of layer 6, u_1 represents the displacement of layer 1 at the same instant (corresponding to u^{p}_{6}), and y_i denotes the vertical coordinate of the center of layer i.

Figure **9a** shows the calculated cyclic compressive stresses at various depths, obtained for an excitation amplitude of $u_0 = 4 \times 10^{-4} m$ and an angular frequency of 30rad/s.

Figure **9b-d** show the evolution of cyclic compressive stresses in the third, fourth, and fifth layers, respectively.

Figure **10** illustrates the stress–strain hysteresis loops used to estimate the maximum oedometric modulus, E_0, during the steady-state response phase. The data were recorded between 4.5 *seconds* and 10.5 *seconds* for the unconfined soil deposit, thereby ensuring that transient effects were excluded from the analysis.

This figure highlights the nonlinear behaviour and energy dissipation of the granular material. The initial slope defines the maximum oedometric modulus, $E_0 \cong 82.7 \times 10^4\ Pa$.

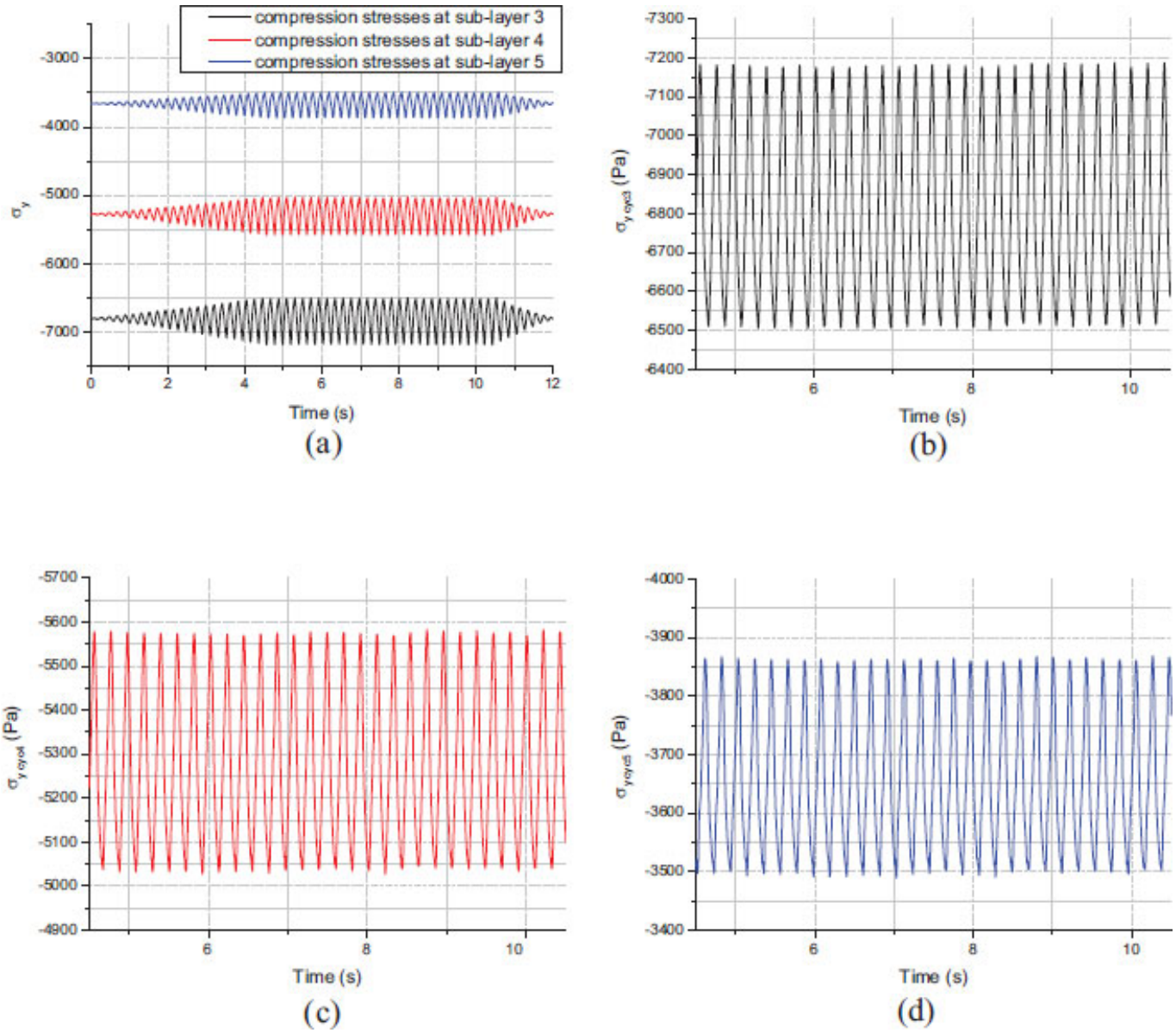


Fig. (9). Evolution of cyclic compressive stresses at various depths within the granular deposit: (**a**) global overview, (**b**) details at the third layer $\sigma_y\ cyc_3$, (**c**) fourth layer $\sigma_y\ cyc_4$, (**d**) fifth layer $\sigma_y\ cyc_5$.

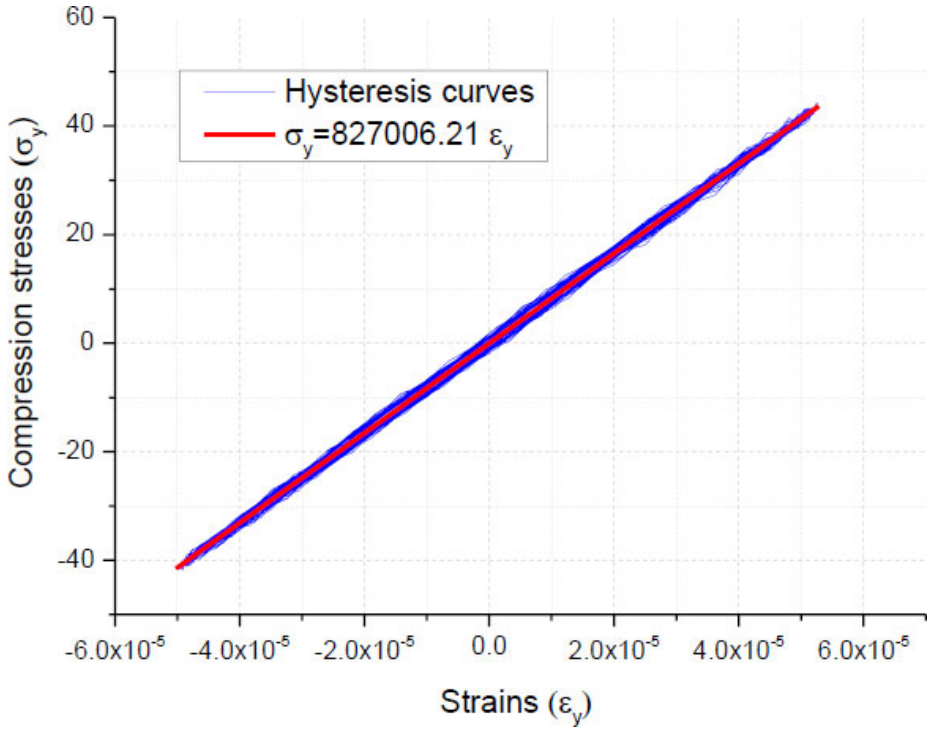


Fig. (10). Hysteresis curves used to estimate the maximum oedometric modulus E_0.

It can be observed that the oedometric modulus obtained from free vibration (Section 3.1) is higher than that derived from the hysteresis loops at low excitation amplitudes. This suggests that the oedometric modulus obtained from free vibration corresponds to the maximum dynamic modulus, $E_0\ max$, measured under predominantly elastic conditions. In contrast, the modulus derived from the hysteresis loops is a secant modulus that accounts for interparticle sliding and energy dissipation. Consequently, even at very low deformation amplitudes, the modulus obtained from free vibration is higher than that derived from hysteresis loops.

The results highlight the significant influence of micromechanical interactions on the dynamic behaviour of granular materials. The discrepancy observed between the oedometric modulus obtained from free vibration and that derived from the hysteresis loops indicates that energy dissipation mechanisms, such as interparticle sliding and friction, play a crucial role even at very low deformation amplitudes.

3.3. Effect of Confinement Pressure on Oedometric Modulus Estimation (E_0)

In order to study the oedometric modulus of a deep soil layer, a weighted chain of grains is introduced at the surface of the deposit; the confining stress can be increased by increasing the specific weight of the grains forming the chain. In this analysis, the deposit is subjected to a harmonic excitation with $u_0 = 4 \times 10^{-4} m$, a frequency of 30rad/s and confining pressures of 10 kPa and 20 kPa.

Figure **11a** and **b** illustrate the influence of confining pressure on the estimation of the maximum oedometric modulus E_0.

Figure **11** shows that the soil profile subjected to a low confining pressure (a) exhibits a lower oedometric modulus than the profiles subjected to higher confining pressures (b), confirming the influence of confining pressure on soil stiffness. This finding highlights the role of confinement in determining the mechanical behaviour of the soil and the load-bearing capacity of the granular medium. Overall, increasing the confining pressure leads to a noticeable increase in stiffness, consistent with well-established geotechnical principles.

3.4. Oedometric Modulus Degradation

This section investigates the degradation of the oedometric modulus within the unconfined sand profile under increasing excitation amplitudes. The analysis is conducted at a constant angular frequency of 30 rad/s, with amplitudes ranging from $4 \times 10^{-5} m$ to $4 \times 10^{-3} m$. Figure **12** illustrates the influence of excitation amplitude on both the oedometric modulus, E, and the displacement time history.

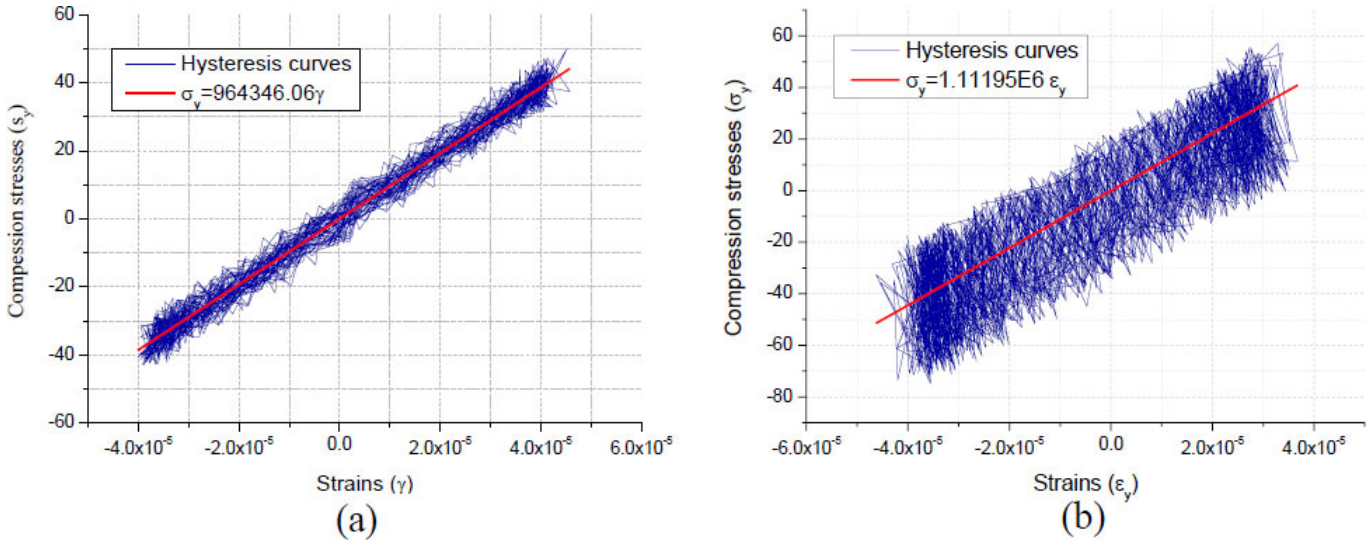


Fig. (11). Influence of confining pressure on the estimation of oedometric modulus E_0: (**a**) $P = 10\ kPa$, (**b**) $P = 20\ kPa$.

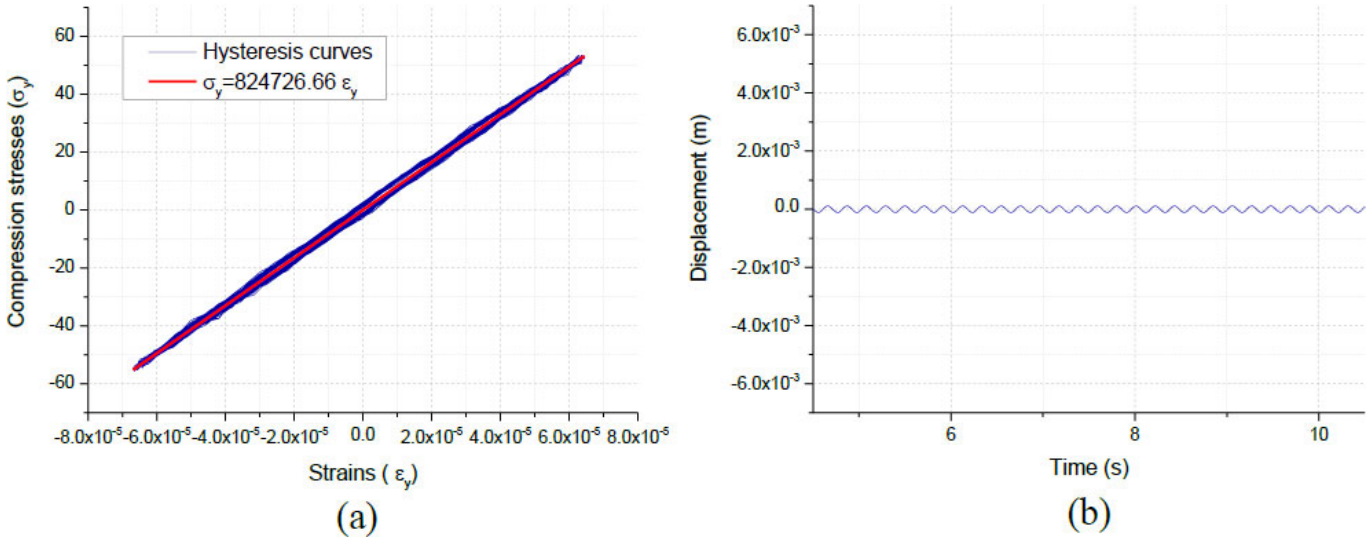


Fig. (12). Dynamic response at the top layer of the sand deposit: (**a**) Hysteresis loops; (**b**) displacement time histories under excitation amplitudes of $u_0 = 1\times10^{-4}$m

3.4.1. Discussion of Oedometric Modulus Degradation amplitudes (≤ 1 × 10^{-4} m), stress-strain

Figure **12** illustrates that at low excitation amplitudes (≤ 1 × 10^{-4} *m*), stress-strain hysteresis loops are virtually absent. This response indicates that the granular assembly remains within a quasi-elastic regime, where energy dissipation is negligible. However, as the excitation amplitude increases, the induced strain within the deposit also increases, triggering the formation and progressive development of well-defined hysteresis loops. The enclosed area of these loops increases with increasing strain, reflecting a clear rise in frictional energy dissipation. From a micromechanical perspective, this transition from predominantly elastic behaviour to frictional energy dissipation is associated with the onset of localised inter-particle sliding and changes in the contact network. This mechanism is consistent with the cyclic DEM findings [14] and the wave attenuation mechanisms reported previously [15].

Furthermore, Figures **12a**, **13a**, **14a**, **15a**, **16a**, and **17a** highlight the progressive degradation of the oedometric modulus (E) as a function of strain amplitude. For an initial excitation amplitude of 1×10^{-4} *m*, the computed oedometric modulus is approximately $82{,}47\times10^{4}$

Pa. Increasing the excitation amplitude to 1×10^{-3} *m* induces a significant decrease in the modulus to $71{,}77 \times 10^{4}$ *Pa*, demonstrating the nonlinear degradation of the oedomertic modulus under dynamic loading at larger strain amplitudes. This reduction in stiffness is evidenced by the decreasing slope of the hysteresis loops. This macroscopic stiffness degradation is associated with the rearrangement of grain contacts and changes in the granular fabric. Such changes may be influenced by particle shape and accompanied by a redistribution of contact forces within the granular assembly, ultimately affecting its overall mechanical response.

This dynamic softening is further corroborated by the displacement time histories shown in Figures **12b**, **13b**, **14b**, **15b**, **16b**, and **17b**. An examination of the steady-state wave propagation through the specimen shows that the displacement amplification factor in the upper soil layer (defined as the ratio of the surface displacement amplitude to the prescribed bedrock displacement amplitude) increases from 1.13 at an excitation amplitude of 1×10^{-4} *m* to a much higher value of 1.43 at an excitation amplitude of 1×10^{-3} *m*.

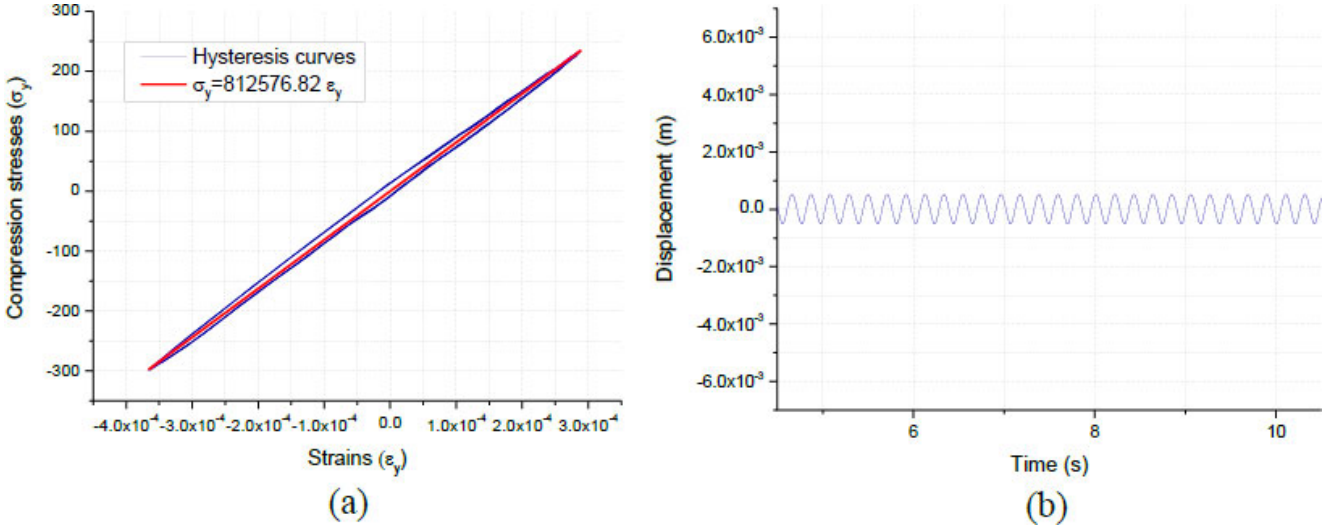


Fig. (13). Dynamic response at the top layer of the sand deposit: (**a**) Hysteresis loops; (**b**) displacement time histories under excitation amplitudes of $u_0 = 1 \times 10^{-4}$m.

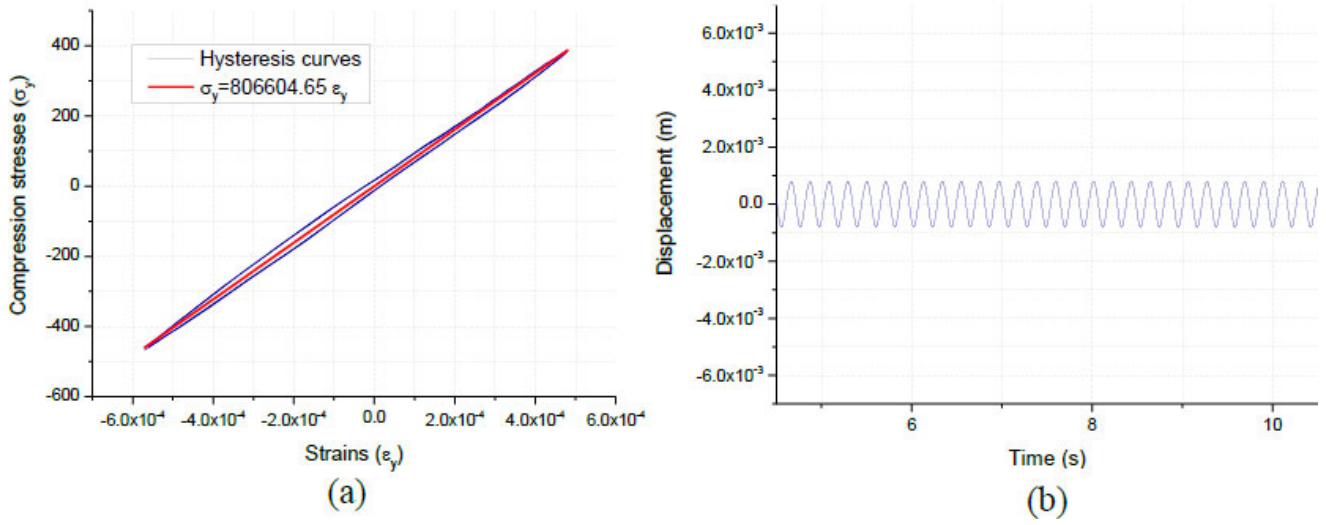


Fig. (14). Dynamic response at the top layer of the sand deposit: (**a**) Hysteresis loops; (**b**) displacement time histories under excitation amplitudes of $u_0 = 6 \times 10^{-4}$m.

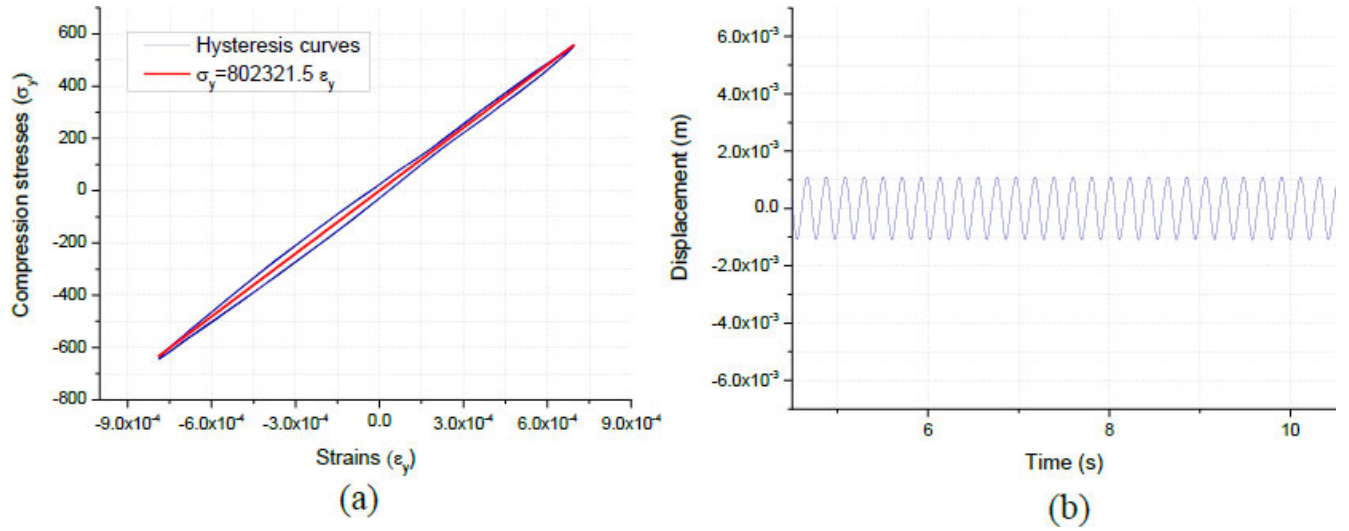


Fig. (15). Dynamic response at the top layer of the sand deposit: (**a**) Hysteresis loops; (**b**) displacement time histories under excitation amplitudes of $u_0 = 8\times10^{-4}$m.

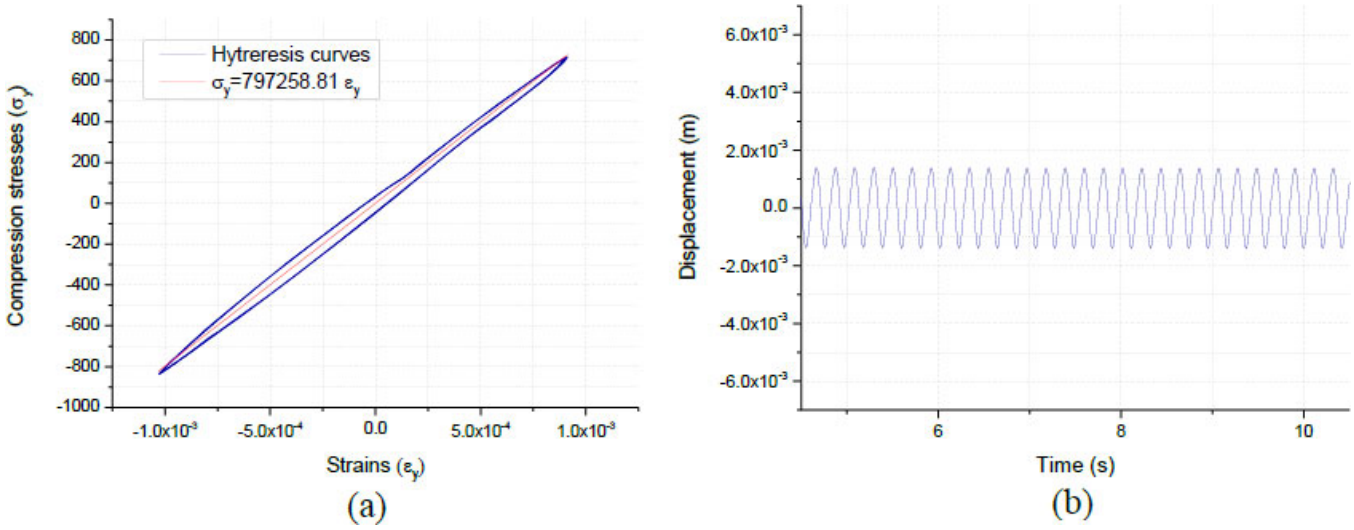


Fig. (16). Dynamic response at the top layer of the sand deposit: (**a**) Hysteresis loops; (**b**) displacement time histories under excitation amplitudes of 1×10^{-3}m.

This increase in surface displacement amplification provides additional macroscopic evidence of the reduction in stiffness. As the material's stiffness degrades, its dynamic response becomes increasingly nonlinear, potentially leading to greater deformation and increased energy dissipation.

In Figure **18**, the degradation of the oedometric modulus obtained from the DEM simulation is compared with the reference shear modulus degradation curve [26] and the experimental degradation curves reported in the literature [27, 28].

Figure **18a** shows the progressive degradation of the oedometric modulus as a function of strain amplitude. This degradation is relatively mild and gradual compared with that of the reference shear modulus degradation curve. The difference in the degradation trends between the shear modulus and the oedometric modulus can be attributed to the distinct types of mechanical stiffness represented by these moduli. The shear modulus is associated with resistance to shear deformation, whereas the oedometric modulus is related to the soil's stiffness under vertical compressive loading under constrained lateral conditions. The less pronounced degradation of the oedometric modulus observed in Figure **18a** may reflect the different mechanical responses of the two moduli.

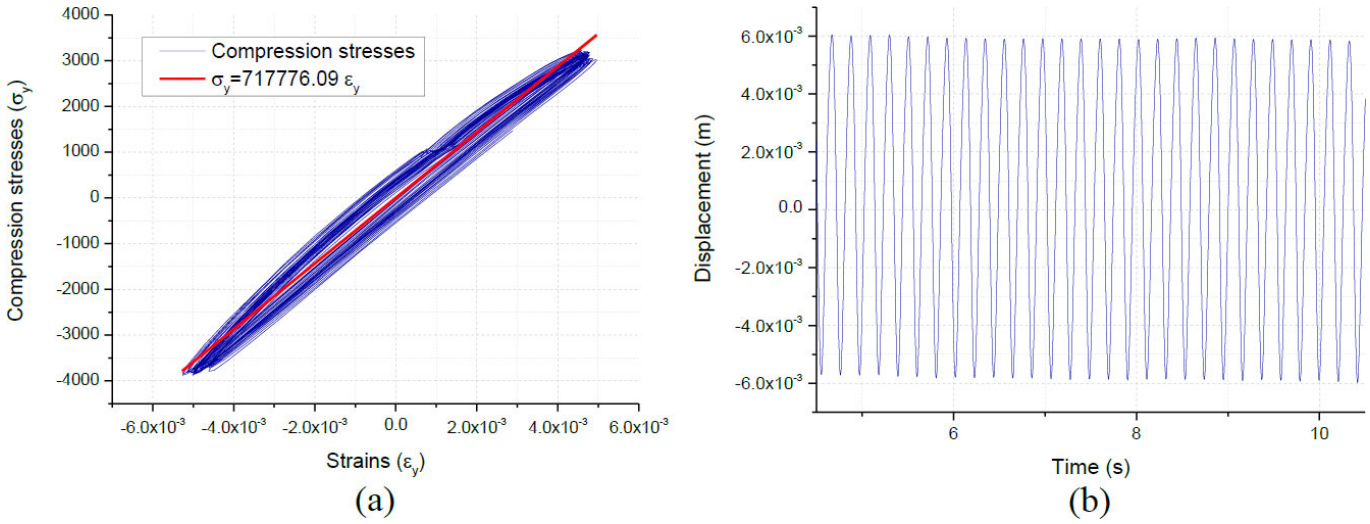


Fig. (17). Dynamic response at the top layer of the sand deposit: (**a**) Hysteresis loops; (**b**) displacement time history under excitation amplitudes of 4×10^{-3}m.

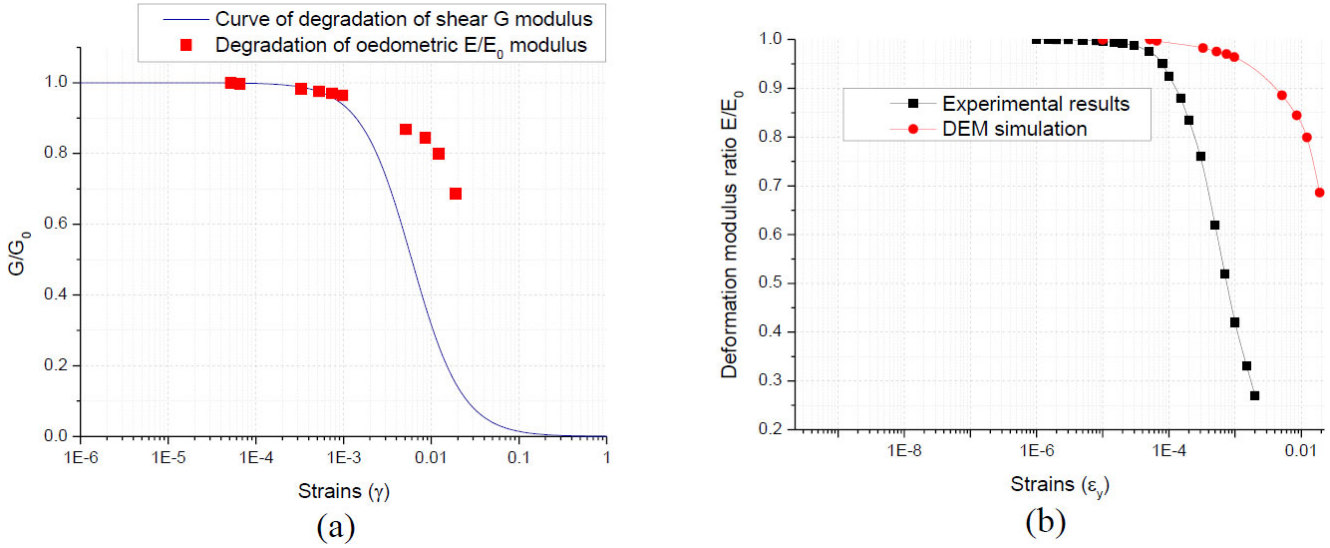


Fig. (18). Oedometric modulus degradation curve E/E_0: (**a**) Comparison with the shear modulus degradation curve [26]; and (**b**) validation against experimental degradation curves [27, 28].

Figure **18b** exhibits a progressive stiffness reduction with increasing deformation, in agreement with the experimental trend reported by [28]. A clear transition from a quasi-linear regime to a nonlinear response is observed at a deformation amplitude of approximately $\gamma \approx 10^{-4}$ which corresponds to the commonly reported threshold for the onset of nonlinearity in granular soils. Although the DEM curve displays slightly more gradual and less pronounced degradation than the experimental reference, the overall trend and the identified transition deformation amplitude support the reliability of the DEM simulations in analysing compression-wave propagation and capturing the main mechanisms governing modulus degradation. Specifically, at very low strain amplitudes, the modulus remains nearly constant, whereas higher strain levels induce nonlinear mechanisms such as interparticle sliding.

3.5. Damping Ratio Evolution (ξ)

The damping ratio (ξ) can be estimated from hysteresis curves by calculating the equivalent damping ratio, which is derived from the area enclosed by the hysteresis loop. In geomechanics and soil dynamics, this parameter is commonly used to characterize the energy dissipation capacity of granular materials subjected to cyclic loading.

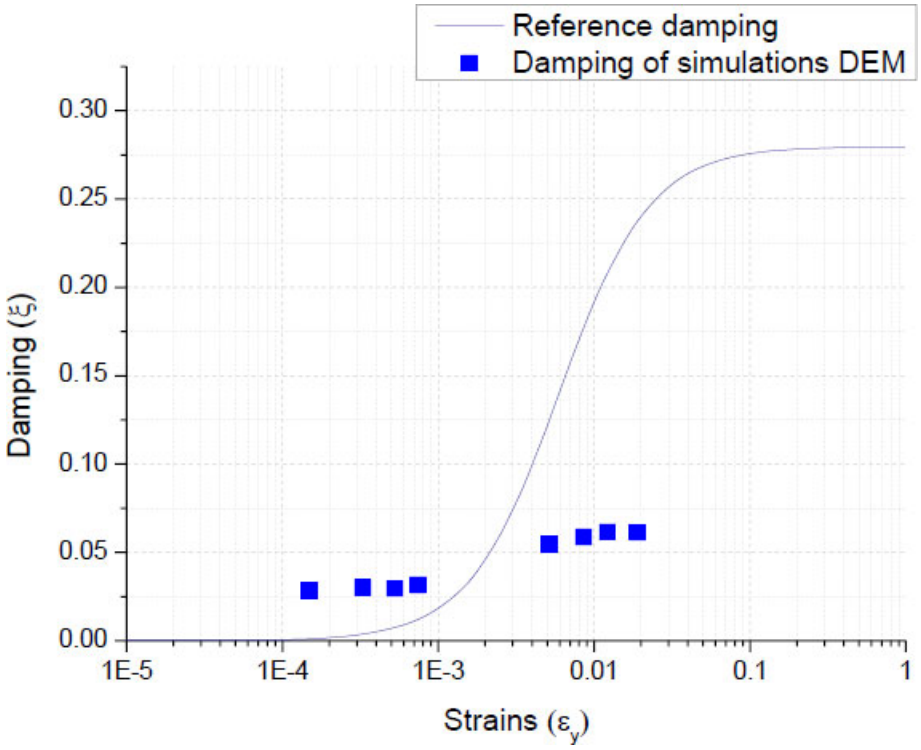


Fig. (19). Variation of the damping ratio ξ.

The equivalent damping ratio is commonly used to characterise the energy dissipation capacity of granular materials subjected to cyclic loading.

The equivalent damping ratio ξ can be determined using the following expression Eq. (**23**):

$$\xi = \frac{1}{4\pi}\frac{\Delta W}{W_e} \quad \textbf{(23)}$$

where:

ΔW denotes the area of the hysteresis loop, representing the energy dissipated by the material during a loading–unloading cycle.

We is the maximum elastic deformation energy stored in the material, corresponding to the area under the secant line associated with the compression modulus E.

4π is a normalisation factor derived from the analogy with a damped harmonic oscillator.

Figure **19** illustrates the comparison between the evolution of the damping ratio (ξ) in the investigated sand profile and the experimental reference curve for shear wave propagation derived experimentally [27].

Figure **19** shows a slight and gradual increase in the damping ratio (ξ) with increasing strain amplitude. Specifically, the damping ratio rises from 0.028 (2.8%) at a strain amplitude of approximately 10^{-4} to 0.0615 (6.15%) at a strain amplitude on the order of 10^{-2}. This trend differs from from the reference shear damping curve, suggesting that the soil profile exhibits lower damping in compression than in shear. This behaviour can be attributed to the differences in the mechanical response and contact mechanisms mobilised during compression and shear loading.

CONCLUSION

In this study, a two-dimensional model of compression wave propagation through a granular material profile is developed using the Discrete Element Method (DEM). The micromechanical response of the granular assembly subjected to harmonic excitations applied at the bedrock was investigated through a series of numerical simulations. The dynamic behaviour of the medium was examined by analyzing several key parameters, including the estimation of the temporal evolution of displacements, motion amplification, oedometric modulus degradation, and variations in the damping ratio.

Furthermore, the oedometric modulus was estimated under low-amplitude excitations and compared with the corresponding values obtained from hysteresis loop analyses. The simulation determined the upper elastic limit *via* free-vibration at 83.8×10^{4} *Pa*, whereas the hysteresis-based secant modulus yielded a lower value of $82.7\times10^{4}Pa$ due to frictional energy dissipation at interparticle contact. The influence of confining pressure on the estimation of the elastic modulus E was also investigated, showing that higher confinement (10 *kPa* and 20 *kPa*) leads to increased stiffness in the soil profile.

The findings confirm the capability and reliability of the Discrete Element Method for simulating compression-

wave propagation in granular media. The simulations demonstrated that the profile exhibits damped elastic behaviour, with motion amplification increasing with excitation amplitude, while confining pressure enhances the stiffness of the granular structure.

The degradation of the oedometric modulus and the variation in the damping ratio were analyzed in depth, revealing the different response phases as a function of the dynamic excitation amplitude. Crucially, the numerical simulations show a clear transition from a quasi-linear regime to a nonlinear response at a strain amplitude of approximately $\gamma \approx 10^{-4}$, which indicates the micromechanical threshold identified in this study for the onset of non-linearity in granular soil [9, 14, 23]. The observed relationship between the reduction of the oedometric modulus and the damping ratio sheds light on the micromechanical origins of the dynamic behavior of granular media. The results of his study demonstrated the ability of the Discrete Element Method (DEM) to reproduce the complex interaction between particle-scale dynamics and the macroscopic behavior of granular media subjected to compression-wave propagation.

It is essential to point out certain limitations of the current model. First, the use of idealised 2D circular particles inevitably neglects the complex geometric characteristics of angular and naturally shaped soil grains. Furthermore, this approach, which focuses on one-dimensional compression under oedometric conditions, does not allow for the consideration of multidirectional stress paths or the formation of localised shear bands. Clearly identifying these limitations is a crucial step in guiding future extensions towards fully three-dimensional (3D) simulation of soil dynamics.

AUTHORS' CONTRIBUTIONS

The authors confirm their contribution to the paper as follows: S.D.: Contributed to the conception, writing, review, and editing of the manuscript, and developed the C++ code; H.A.: Participated in writing and reviewing the manuscript. All authors reviewed the results and approved the final version of the manuscript.

LIST OF ABBREVIATIONS

DEM = Discrete Element Method

2D = Two-Dimensional

3D = Three-Dimensional

C++ = An extension of the C programming language with object–oriented features

CONSENT FOR PUBLICATION

Not applicable.

AVAILABILITY OF DATA AND MATERIALS

Data will be made available on request.

FUNDING

None.

CONFLICT OF INTEREST

The authors declare no conflict of interest, financial or otherwise.

ACKNOWLEDGEMENTS

Declared none.

APPENDIX: Table of symbols.

Symbol	Definition	Unit
$\vec{x}_i$	Position vector	m
$\ddot{\vec{x}}_i$	Acceleration vector	m/s^2
φ_i	Rotation vector	rad
$\ddot{\vec{\varphi}}_i$	Angular acceleration	rad/s^2
m_i	Mass	kg
I_i	Moment of inertia	Kg.m^2
$\vec{F}_{ij}^{contact}$	Contact force	N
$\vec{F}_n$	Normal contact force	N
$\vec{F}_s$	Tangential contact force	N
D_n	Normal overlap	m
D_s	Tangential displacement	m
V_n	Normal relative velocity	m/s
V_s	Tangential relative velocity	m/s
k_n	Normal stiffness	N/m
k_s	Tangential stiffness	N/m
ν_n	Normal damping coefficient	kg/s
ν_s	Tangential damping coefficient	kg/s
μ_s	Static friction coefficient	–
μ_d	Dynamic friction coefficient	–
M_r	Rolling resistance moment	N.m
$u(z, t)$	Displacement	m

Symbol	Definition	Unit
u_0	Excitation amplitude	m
ω	Angular frequency	rad/s
E	Oedometric modulus	Pa
E_0	Maximum oedometric modulus	Pa
$\sigma_{y\,cyc}$	Vertical cyclic stress	Pa
$\varepsilon_{y\,cyc}$	Vertical cyclic strain	-
ξ	Damping ratio	%
ρ	Density	kg/m^3
h	Soil layer depth	m

REFERENCES

[1] J.D. Goddard, "Continuum modeling of granular media", *Appl. Mech. Rev.,* vol. 66, no. 5, p. 050801, 2014. [http://dx.doi.org/10.1115/1.4026242]

[2] J.M. Ting, M. Khwaja, L.R. Meachum, and J.D. Rowell, "An ellipse-based discrete element model for granular materials", *Int. J. Numer. Anal. Methods Geomech.,* vol. 17, no. 9, pp. 603-623, 1993. [http://dx.doi.org/10.1002/nag.1610170902]

[3] I.S. Aranson, and L.S. Tsimring, "Patterns and collective behavior in granular media: Theoretical concepts", *Rev. Mod. Phys.,* vol. 78, no. 2, pp. 641-692, 2006. [http://dx.doi.org/10.1103/RevModPhys.78.641]

[4] X. Tang, and J. Yang, "Wave propagation in granular material: What is the role of particle shape?", *J. Mech. Phys. Solids,* vol. 157, p. 104605, 2021. [http://dx.doi.org/10.1016/j.jmps.2021.104605]

[5] Q.W. Ma, Y. Sandali, R.N. Zhang, F.Y. Ma, H.T. Wang, S.P. Ma, and Q.F. Shi, "Characterization of elastic modulus of granular materials in a new designed uniaxial oedometric system", *Chin. Phys. B,* vol. 33, no. 3, p. 038101, 2016. [http://dx.doi.org/10.1088/0256307X/33/3/038101]

[6] C.J. Hsu, D.L. Johnson, R.A. Ingale, J.J. Valenza, N. Gland, and H.A. Makse, "Dynamic effective mass of granular media", *Phys. Rev. Lett.,* vol. 102, no. 5, p. 058001, 2009. [http://dx.doi.org/10.1103/PhysRevLett.102.058001] [PMID: 19257558]

[7] A. Ozbay, and A.F. Cabalar, "Effects of triaxial confining pressure and strain rate on stick-slip behavior of a dry granular material", *Granul. Matter,* vol. 18, no. 3, p. 60, 2016. [http://dx.doi.org/10.1007/s10035-016-0664-7]

[8] A.T. Gezgin, B. Soltanbeigi, and O. Cinicioglu, "Discrete-element modelling of pile penetration to reveal influence of soil characteristics", *Geotech. Eng.,* vol. 175, no. 4, pp. 365-382, 2022. [http://dx.doi.org/10.1680/jgeen.20.00134]

[9] C. Arda, and O. Cinicioglu, "Influence of grain shape on stress-dilatancy parameters", *Granul. Matter,* vol. 23, no. 2, p. 22, 2021. [http://dx.doi.org/10.1007/s10035-021-01098-2]

[10] Z. Cheng, B. He, D. Xu, X. Fan, and H. Shen, "A CFD-DEM study on seepage erosion and pore-structure evolution in gap-graded soils with irregular grain shapes", *Powder Technol.,* vol. 122073, 2025. [http://dx.doi.org/10.1016/j.powtec.2025.122073]

[11] C. Guo, C. Zhou, M.A. Meguid, and P. Tai, "DEM modelling of the axial behaviour of underground pipelines buried in unsaturated coarse-grained soils", *Comput. Geotech.,* vol. 196, p. 108122, 2026. [http://dx.doi.org/10.1016/j.compgeo.2026.108122]

[12] P. Cui, T. Su, L. Liu, T. Wang, B. Li, X. Guan, and X. Mei, "Characteristics of compression wave propagation and energy absorption effects in dry sandy soil", *Sci. Rep.,* vol. 14, no. 1, p. 31625, 2024. [http://dx.doi.org/10.1038/s41598-024-80525-9] [PMID: 39738193]

[13] Y. Li, M. Otsubo, and R. Kuwano, "DEM analysis on the stress wave response of spherical particle assemblies under triaxial compression", *Comput. Geotech.,* vol. 133, p. 104043, 2021. [http://dx.doi.org/10.1016/j.compgeo.2021.104043]

[14] A. Ezzeddine, B. Cazacliu, P. Richard, L. Thorel, and R. Artoni, "A discrete element study on sand response to cyclic loading: Macro-micro perspectives", *Granul. Matter,* vol. 26, no. 4, p. 101, 2024. [http://dx.doi.org/10.1007/s10035-024-01467-7]

[15] T. Mohamed, J. Duriez, G. Veylon, L. Peyras, and P. Soulat, "A discrete-based multi-scale modeling approach for the propagation of seismic waves in soils", *Soil. Dyn. Earthquake Eng.,* vol. 173, p. 108104, 2023. [http://dx.doi.org/10.1016/j.soildyn.2023.108104]

[16] T. Pöschel, and T. Schwager, *Computational Granular Dynamics: Models and Algorithms,* Springer-Verlag: Berlin Heidelberg, Germany, 2005. [http://dx.doi.org/10.1007/3-540-27720-X]

[17] P.A. Cundall, and O.D.L. Strack, "A discrete numerical model for granular assemblies", *Geotechnique,* vol. 29, no. 1, pp. 47-65, 1979. [http://dx.doi.org/10.1680/geot.1979.29.1.47]

[18] V. Richefeu, "*3D discrete element approach to the behavior of low-stress cohesive granular materials*", Doctor of Philosophy, University of Montpellier, 2005.

[19] M. Fakih, J.Y. Delenne, F. Radjai, and T. Fourcaud, "Root growth and force chains in a granular soil", *Phys. Rev. E,* vol. 99, no. 4, p. 042903, 2019. [http://dx.doi.org/10.1103/PhysRevE.99.042903] [PMID: 31108586]

[20] J.Y. Delenne, M.S. El Youssoufi, F. Cherblanc, and J.C. Bénet, "Mechanical behaviour and failure of cohesive granular materials", *Int. J. Numer. Anal. Methods Geomech.,* vol. 28, no. 15, pp. 1577-1594, 2004. [http://dx.doi.org/10.1002/nag.401]

[21] J. Wang, and X. Chu, "Compressive wave propagation in highly ordered granular media based on DEM", *Int. J. Nonlinear Sci. Numer. Simul.,* vol. 19, no. 5, pp. 545-552, 2018. [http://dx.doi.org/10.1515/ijnsns-2017-0213]

[22] A. Verruijt, *An Introduction to Soil Dynamics,* Springer Science Business Media, Springer: Dordrecht, Netherlands, 2009. [http://dx.doi.org/10.1007/978-90-481-3441-0]

[23] S. Derbane, M. Mansouri, S. Messast, and A. El Malki Alaoui, "On the behavior of a granular soil deposit subjected to horizontal vibration. A discrete element modeling", *C. R. Mec.,* vol. 353, no. G1, pp. 321-338, 2025. [http://dx.doi.org/10.5802/crmeca.282]

[24] S. Luding, "Cohesive, frictional powders: Contact models for tension", *Granul. Matter,* vol. 10, no. 4, pp. 235-246, 2008. [http://dx.doi.org/10.1007/s10035-008-0099-x]

[25] N. Zamani, and U. El Shamy, "Analysis of wave propagation in dry granular soils using DEM simulations", *Acta Geotech.,* vol. 6, no. 3, pp. 167-182, 2011. [http://dx.doi.org/10.1007/s11440-011-0142-7]

[26] "French Committee of Soil Mechanics and Geotechnical Engineering (CFMS)", Available from: https://www.cfms-sols.org/

[27] T. Iwasaki, F. Tatsuoka, and Y. Takagi, "Shear moduli of sands under cyclic torsional shear loading", *Soils Found.,* vol. 18, no. 1,

pp. 39-56, 1978.
[http://dx.doi.org/10.3208/sandf1972.18.39]

[28] T. Kokusho, "Cyclic triaxial test of dynamic soil properties for wide strain range", *Soil Found.*, vol. 20, no. 2, pp. 45-60, 1980.
[http://dx.doi.org/10.3208/sandf1972.20.2_45]

[29] S. Derbane, H. Ayas, and M. Mansouri, "Dynamic response of a cracked structure influenced by micromechanical parameters of sand supporting", *Struct. Integr. Life,* vol. 26, no. 1, pp. 164-170, 2026.
[http://dx.doi.org/10.69644/ivk-2026-01-0164]

DISCLAIMER: Please note that this article is currently in the 'Early view' stage and is not the final 'Version of Record'. While it has been accepted, copy-edited, and formatted, however, it is still undergoing proofreading and corrections by the authors. Therefore, the text may still change before the final publication. Although 'Early view' may not have all bibliographic details available, the DOI and the year of online publication can still be used to cite them. The article title, DOI, publication year, and author(s) should all be included in the citation format. Once the 'Final Version of Record' becomes available the 'Early view' will be replaced by that.